Steady-State Kinetic Characterization of Substrates and Metal-Ion Specificities of the Full-Length and N-Terminally Truncated Recombinant Human Methionine Aminopeptidases (Type 2)

Guang Yang,*,‡ Robert B. Kirkpatrick,§ Thau Ho,§ Gui-Feng Zhang,§ Po-Huang Liang,§,|| Kyung O. Johanson,§ David J. Casper,⊥ Michael L. Doyle,⊥,# Joseph P. Marino, Jr.,@ Scott K. Thompson,@ Wenfang Chen,‡ David G. Tew,‡ and Thomas D. Meek‡

Departments of Assay Methodology Development, Gene Expression and Protein Biochemistry, Computational, Analytical and Structural Sciences, and Medicinal Chemistry, GlaxoSmithKline Pharmaceuticals, 709 Swedeland Road, King of Prussia, Pennsylvania 19406

Received April 20, 2001; Revised Manuscript Received July 18, 2001

ABSTRACT: The steady-state kinetics of a full-length and truncated form of the type 2 human methionine aminopeptidase (hMetAP2) were analyzed by continuous monitoring of the amide bond cleavage of various peptide substrates and methionyl analogues of 7-amido-4-methylcoumarin (AMC) and *p*-nitroaniline (pNA), utilizing new fluorescence-based and absorbance-based assay substrates and a novel coupled-enzyme assay method. The most efficient substrates for hMetAP2 appeared to be peptides of three or more amino acids for which the values of k_{cat}/K_m were approximately 5×10^5 M^{-1} min^{-1}. It was found that while the nature of the P1′ residue of peptide substrates dictates the substrate specificity in the active site of hMetAP2, the P2′ residue appears to play a key role in the kinetics of peptidolysis. The catalytic efficiency of dipeptide substrates was found to be at least 250-fold lower than those of the tripeptides. This substantially diminished catalytic efficiency of hMetAP2 observed with the alternative substrates MetAMC and MetpNA is almost entirely due to the reduction in the turnover rate (k_{cat}), suggesting that cleavage of the amide bond is at least partially rate-limiting. The 107 N-terminal residues of hMetAP2 were not required for either the peptidolytic activity of the enzyme or its stability. Steady-state kinetic comparison and thermodynamic analyses of an N-terminally truncated form and full-length enzyme yielded essentially identical kinetic behavior and physical properties. Addition of exogenous Co(II) cation was found to significantly activate the full-length hMetAP2, while Zn(II) cation, on the other hand, was unable to activate hMetAP2 under any concentration that was tested.

Human methionine aminopeptidase (type 2) (hMetAP2),[1] an apparent cobalt(II)-containing exopeptidase, catalyzes the removal of the amino-terminal methionine from newly translated polypeptides. Inactivation of the hMetAP2 activity in endothelial cells by fumagillin and other inactivators has been shown to effectively block the proliferation of these cells (*14*, *33*, *37*). Since endothelial proliferation permits extension of the microvascular tubules (angiogenesis), a process apparently critical to the neovascularization and metastasis of tumors (*12*, *18*, *27*, *28*), the specific inhibition of human MetAP2 constitutes a promising new target for cancer chemotherapy.

The first report of mammalian type 2 methionine aminopeptidase described an enzyme that was copurified with the eukaryotic initiation factor 2α (eIF-2α) from rabbit reticulocyte lysates as a 67 kDa polypeptide (*15*). Subsequently, the genes of human and rat MetAP2 have since been cloned, and the protein sequences comprise a unique N-terminal region containing one aspartate-rich region and two lysine-rich regions, and a conserved C-terminal catalytic domain with a novel protease fold, termed the "pita bread" fold (*2*, *3*, *22*, *39*). The amino acid sequences of the human and rat MetAP2 are 92% identical.

The catalytic pita bread fold, which resides in a deep cleft in the C-terminal region of the MetAP enzymes, appears to be conserved in all MetAP enzymes, in prolidase, in aminopeptidase P, and also in the related enzyme, creatinase

* To whom correspondence should be addressed. E-mail: guang_yang@sbphrd.com. Fax: (610) 270-4074.

‡ Department of Assay Methodology Development.

§ Department of Gene Expression and Protein Biochemistry.

|| Present address: Institute of Biological Chemistry, Academia Sinica, Nankang, Taipei 115, Taiwan.

⊥ Department of Computational, Analytical and Structural Sciences.

Present address: Biopharmaceutical Sciences & Technologies H13-07, Bristol-Myers Squibb PRI Pharmaceutical Research Institute, P.O. Box 4000, Princeton, NJ 08543-4000.

@ Department of Medicinal Chemistry.

[1] Abbreviations: hMetAP2, human methionine aminopeptidase (type 2); eIF-2α, eukaryotic initiation factor 2; M(II) or M^{2+} (M = Co, Mg, Mn, or Zn), divalent metal cation; AAO, L-amino acid oxidase; HRP, horseradish peroxidase; Met-pNA, L-methionine *p*-nitroanilide; Met-AMC, L-methionine 7-amido-4-methylcoumarin; L-Nle, L-norleucine; HTS, high-throughput screening; λ_{ex}, excitation wavelength; $\Delta\epsilon$, extinction coefficient change; CD, circular dichroism; MALDI-MS, matrix-assisted laser desorption/ionization mass spectrometry; ICP, inductively coupled plasma; IC_{50}, inhibitor concentration at which enzyme is 50% inhibited; Gnd-HCl, guanidinium hydrochloride; AEBSF, 4-(2-aminoethyl)benzenesulfonyl fluoride, a water soluble, covalent inhibitor of serine proteases.

10.1021/bi010806r CCC: $20.00
Published on Web 08/11/2001

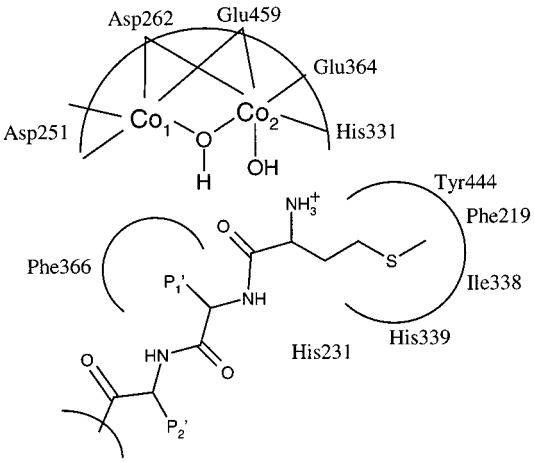

FIGURE 1: Schematic view of a hypothetical model of an N-terminal methionyl peptide in the binding pocket of human methionine aminopeptidase type 2, based on the crystal structures of apo-hMetAP2 and the hMetAP2−fumagillin complex (*23*). Each arch curve represents the binding pocket for the metal ion (cobalt, Co_1 and Co_2) center, the methionine side chain, and the P1′ side chain. Residues in the active site of hMetAP2 defining each pocket are listed near each arch. The bonds between two cobalt ions and five active site residues indicate either a bidentate or a monodentate coordination of each residue in metal ion chelation. HO represents the metal-bound water molecule (or ion) in the active site of hMetAP2. P_1' and P_2' represent the side chains of amino acids at position P_1' and P_2' of a peptide.

(*3*, *23*, *34*). The crystal structure study of hMetAP2 and its fumagillin complex (*23*) suggested that a completely covered pocket near the active site occupied by the epoxide-bearing side chain of fumagillin is most likely the binding pocket of the methionine side chain (see Figure 1). A 64-amino acid sequence insertion (from residue 381 to 444 in hMetAP2) in the catalytic domain distinguishes the MetAP2 family from the MetAP1 family. Preliminary kinetic characterization of hMetAP2 (*22*) indicated that like other MetAPs, hMetAP2 catalyzes a Co(II)-dependent cleavage of the N-terminal methionine with a stringent substate specificity, which is apparently dictated by the steric nature of the P1′ residue (gyration radius of <1.29 Å; *5*, *17*, *32*). Recent studies with the type 1 yeast methionine aminopeptidase (*36*) and the *Escherichia coli* methionine aminopeptidase (*9*) suggested that Zn(II) and Fe(II) cations, respectively, could be the metal ions utilized in vivo. It has been further suggested recently that the *E. coli* MetAP enzyme could function as a mononuclear metalloprotease (*10*).

The N-terminal extension of MetAP enzymes differentiates the methionine aminopeptidases in eukaryotes from those in eubacteria. For yeast methionine aminopeptidase (Type 1), its N-terminal extension (zinc finger domain) was shown not to be required for the methionine aminopeptidase activity (*41*). The N-terminally truncated yeast MetAP1 enzyme exhibited essentially the same K_m and k_{cat} values as the full-length enzyme. The highly charged N-terminal extension in mammalian MetAP2 enzymes has been speculated to be only involved in the binding of eIF-2α to prevent phosphorylation of this factor (*15*). Inactivation of the catalytic activity of hMetAP2 by ovalicin, fumagillin, and TNP470 (a fumagillin analogue) did not affect protection of eIF-2α from phosphorylation by cellular enzymes (*14*), suggesting that the active site responsible for peptidolysis is functionally distinct from the subsite which binds eIF-2α.

Despite the progress in the structural and chemical approaches to understanding the chemical mechanism of this enzyme (*23*, *24*), detailed and systematic kinetic analysis remains preliminary to date. Herein, we report the steady-state kinetic characterization of both the full-length enzyme and a truncated isoform of hMetAP2 which lacks the 107 N-terminal residues of hMetAP2, and an analysis of substrate specificities of these enzyme forms. We found that the exogenous addition of divalent metal ions (including divalent cobalt) ablates hMetAP2 activity. Zn(II) apparently is not the kinetically relevant metal cofactor for the type 2 human methionine aminopeptidase enzyme.

MATERIALS AND METHODS

General. Enzyme assays were carried out on either a conventional spectrophotometer or a 96-well fluorescence plate reader. For fluorescence emission, a Fluorolog-3 spectrofluorometer equipped with a DataMax operation system (Instruments S. A., Inc.) and a Cytofluor Series 4000 multiwell plate reader (PerSeptive Biosystems) or a SpectraMAX Gemini plate reader (Molecular Devices) were used. Spectrophotometric assays were measured using either a *Vectra* XA UV−vis spectrometer (Hewlett-Packard) or a SPECTRAmax microplate spectrophotometer with the SOFTmax PRO operation system (Molecular Devices). All chemicals that were used were of the highest commercially available quality (Sigma, Bachem, and others). Polyclonal antibodies based on peptide epitopes derived from hMetAP2 were prepared by Research Genetics, Inc. (Birmingham, AL) using epitope sequences from both the N-terminal and C-terminal regions of the enzyme.

Subcloning and Overexpression of hMetAP2. A fetal endothelial cell-derived *EST* clone encoding full-length hMetAP2 (GenBank accession number 296441; TIGR THC entry THC171071) was obtained from American Type Culture Collection (Rockville, MD). The complete sequence of the *p*Bluescript insertion was confirmed by automated dideoxy sequencing (Applied Biosystems, Foster City, CA). The complete coding sequence was then subcloned on an *Eco*RI−*Hin*dIII restriction fragment into the *p*Fastbac-1 donor plasmid (Life Technologies, Gaithersburg, MD) between the same restriction sites, placing it under the regulation of the baculovirus polyhedrin promoter. Sequence confirmation of the resultant construct, MAP2*p*FB, was performed across cloning junctions.

Recombinant hMetAP2 was expressed in Sf9 cells using the Bac-To-Bac Baculovirus expression system (Life Technologies). The Mini-Tn7 element-directed polyhedrin promoter-driven expression cassette (element) was transposed into bacmid bMON14272 using *E. coli* DH10Bac according to the manufacturer's protocols. Transfection of Sf9 cells with recombinant bacMids resulted in the production of recombinant baculovirus capable of expressing recombinant hMetAP2 in Sf9 cells. Approximately 6 mg of purified, active enzyme was recovered per cell pellet from 1 L of infected cell culture harvested 3 days postinfection (see the purification methods described below).

Purification of Full-Length Recombinant hMetAP2. The full-length hMetAP2 enzyme was purified using a modification of the procedure of Li and Chang (*22*). The cell pastes (from the previous section) were resuspended in a lysis buffer

containing 10 mM Hepes (pH 7.4), 0.5 mM $CoCl_2$, 10% glycerol, 1.5 mM $MgCl_2$, 100 mM KCl, and protease inhibitors (1 μg/mL aprotinin, 1 μg/mL leupeptin, 0.7 μg/mL pepstatin A, and 1 mM AEBSF) and disrupted with a Dounce homogenizer on ice. The lysate was centrifuged at 30000*g* for 30 min, and the supernatant fractions of the cell-free extracts were loaded onto a Source-15 S column (Pharmacia) equilibrated with buffer A [10 mM Hepes (pH 7.4), 0.5 mM $CoCl_2$, and 10% glycerol]. Active fractions from the Source-15 S purification step were then further purified using a Source-15 Q column (Pharmacia). The enzyme activity was monitored using the uncoupled direct assay method described below. A gradient of NaCl (from 100 to 500 mM) in buffer A was used in both columns to elute the active enzyme. A typical yield of 6 mg of pure hMetAP2 (>90% pure judging by the SDS−PAGE gel) was obtained per liter of cell culture.

Purification of Truncated Recombinant hMetAP2. It was found that prolonged incubation of the full-length hMetAP2 in the elution buffer of the first Source-15 S cation exchange column in the absence of protease inhibitors resulted in various proteolytic products of hMetAP2. These major truncated products were proteins with apparent molecular masses of 43 kDa (estimated by SDS−PAGE). N-Terminal sequencing of the 43 kDa protein fragment excised from an SDS−PAGE gel was consistent with a sequence corresponding to an N-terminus at Gly-108 of the predicted sequence of full-length hMetAP2 (^{108}GPRVQTVDPPS). Western analyses using the hMetAP2 specific polyclonal antipeptide (both N-terminal and C-terminal epitope sequence) antibodies confirmed that the 43 kDa protein is a truncated form of hMetAP2 in which the N-terminal region has been removed. The truncated hMetAP2 was found to no longer bind to the Source-15 Q column used in the purification of the full-length enzyme, suggesting that an anionic (acidic) region of the protein had been removed.

To purify the truncated hMetAP2, cell-free extracts containing recombinant full-length hMetAP2 were first subjected to the Source-15 S column purification in the absence of protease inhibitors using the same chromatographic conditions described above. The combined fractions containing full-length hMetAP2 were then incubated at 4 °C for 5 days to allow protease digestion in situ for removal of the first 107 amino acids at the N-terminus and generation of the 43 kDa truncated hMetAP2 (the extent of cleavage was monitored by SDS−PAGE). The mixture containing the truncated protein was next purified using a Superdex G-75 size exclusion column [prepacked Pharmacia HiLoad 26/60, 2.6 cm (diameter) × 60 cm (length)] equilibrated in buffer A. The truncated hMetAP2 was eluted with buffer composed of 10 mM Hepes (pH 7.4), 10% glycerol, and 0.5 mM $CoCl_2$ at a flow rate of 2 mL/min, which yielded 90% pure truncated hMetAP2. Five milligrams of purified enzyme was typically obtained per liter of cultured cells.

Equilibrium Sedimentation and Circular Dichroism. Sedimentation equilibrium data were measured on a Beckman XL-A analytical ultracentrifuge at 20 °C. Samples of pure hMetAP2 at 0.15 mg/mL in buffer containing 5 mM Hepes (pH 7.5) and 100 mM NaCl were applied in double-sector cells equipped with charcoal-filled Epon centerpieces and sapphire windows. The resulting data were fitted to eq 1 (*11*) using the Marquardt−Levenberg nonlinear least-squares algorithm from SigmaPlot (SPSS Science, Chicago, IL).

$$A_i = A_m \exp\left[\frac{M(1-\bar{\nu}\rho)\omega^2(r^2 - r_m^2)}{2RT}\right] + \text{offset} \quad (1)$$

where A_i and A_m are the absorbances of the *i*th data point and at the meniscus, respectively, M is the solution mass of the protein, $\bar{\nu}$ is the partial specific volume of the protein, ρ is the solvent density, ω is the angular velocity in radians per second, r_i and r_m are the radial positions of the *i*th data point and meniscus, respectively, R is the gas constant, T is the absolute temperature, and offset is an offset absorbance that is constant as a function of r_i. In the study presented here, $\rho = 1.005$ g/mL and $\bar{\nu}$ of the hMetAP2 molecules was calculated as 0.73 mL/g using the Sedinterp (version 1.0) program of D. B. Hayes, T. Laue, and J. Philo (University of New Hampshire, Durham, NH).

Circular dichroism (CD) data were measured on a Jasco J-710 CD spectropolarimeter. Samples at approximately 0.2 mg/mL in a 0.1 cm path length water-jacketed cuvette at 20 °C were scanned at a rate of 50 nm/min, and four spectra were averaged in each case. A buffer-only spectrum was subtracted from hMetAP2 spectra, and the resulting ellipticity data, θ (in degrees), were converted to difference molar extinction coefficient data by the relation $\Delta\epsilon = \theta/(32.48lc)$, where l is the path length in centimeters and c is the molarity of hMetAP2 amino acid residues (*38*). The concentration of hMetAP2 was determined by the absorbance at 280 nm using molecular masses of 52 791 and 41 456 Da, and extinction coefficients of 0.872 and 1.11 mL/mg, respectively, calculated (*29*) from the sequence for the full-length and truncated forms. Guanidinium and urea denaturation studies were carried out by incubating the hMetAP2 samples in each final concentration of denaturant for 30 min prior to measuring the extent of unfolding via measurement of the protein ellipticity at 225 nm. The 30 min incubation time was chosen to allow all samples to reach equilibrium.

Synthesis of L*-Norleucine p-Nitroanilide (*L*-Nle-pNA)*. The synthesis of L-Norleucine *p*-nitroanilide was carried out by adaptation of the procedure developed by Rijkers and coworkers (*30*). Accordingly, treatment of the *tert*-butyl oxycarbonyl amino acid with phosphorus oxychloride in pyridine led to amidation by *p*-nitroaniline, and further treatment with HCl in ethyl acetate led to the desired amino acid *p*-nitroanilide (yield of ∼80%). The identity of the compound was established by ^{1}H NMR and mass spectrometry.

Coupled Spectrophotometric Assays of hMetAP2. The methionine aminopeptidase activity of hMetAP2 could be measured spectrophotometrically by monitoring the free l-amino acid formation upon peptidolysis. The release of N-terminal methionine from a tripeptide (Met-Ala-Ser, Sigma) or a tetrapeptide (Met-Gly-Met-Met, Sigma) substrate was assessed by using a coupled enzyme assay comprised of L-amino acid oxidase (AAO) and horseradish peroxidase (HRP) as outlined in eqs 2−4a,b.

$$\text{L-Met-Ala-Ser} \xrightarrow[Co^{2+}]{\text{hMetAP2}} \text{L-Met} + \text{H}_2\text{N-Ala-Ser} \quad (2)$$

$$\text{L-Met} + \text{H}_2\text{O} + \text{O}_2 \xrightarrow{\text{AAO}} \text{2-oxo acid} + \text{NH}_3 + \text{H}_2\text{O}_2 \quad (3)$$

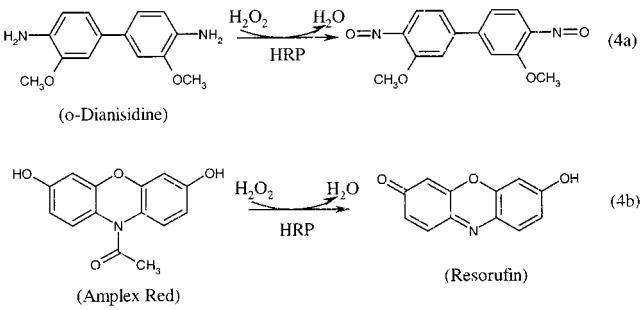

Oxidation by L-amino acid oxidase (AAO, Sigma) (eq 3) of the product methionine (eq 2) generated hydrogen peroxide (H_2O_2). The formation of H_2O_2 was then continuously monitored by its utilization as a substrate for horseradish peroxidase (HRP, Sigma) which then oxidized either *o*-dianisidine (Sigma) (eq 4a) or Amplex Red (Molecular Probes) (eq 4b) as a cosubstrate. Oxidation of *o*-dianisidine was monitored at 30 °C as an increase in absorbance at 450 nm ($\Delta\epsilon = 15\,300$ M^{-1} cm^{-1})[2] in 1 cm path length self-masking cuvettes (*35*). The oxidation of Amplex Red was monitored at 30 °C as an increase in fluorescence emission ($\Delta\epsilon = 54\,000$ M^{-1} cm^{-1}, $\lambda_{ex} = 563$ nm, $\lambda_{ex} = 587$ nm, slit width for excitation and emission = 1.25 mm) (*40*).

In a total volume of 500 μL, a typical assay contained 50 mM Hepes (pH 7.5), 100 mM NaCl, 0.1−1.0 mM $CoCl_2$, 1 mM *o*-dianisidine or 50 μM Amplex Red, 5 units of HRP (Sigma), 1 unit of AAO (Sigma), 10−100 nM hMetAP2, and varying amounts of peptide substrates. The high sensitivity of Amplex Red also allowed the conversion of the coupled enzyme assay into a 96- or 384-well assay format using ≥0.5 nM enzyme in the assay. For a typical 96-well plate assay, the increase in the fluorescence emission ($\lambda_{ex} =$ 563 nm, $\lambda_{em} = 587$ nm) of each well was used to calculate the initial velocity of hMetAP2. Each 50 μL assay contained 50 mM Hepes (pH 7.5), 100 mM NaCl, 0.5−5 nM purified hMetAP2 enzyme, 10 μM $CoCl_2$, 0.5 unit of HRP, 0.04 unit of AAO, 50 μM Amplex Red, and varying amounts of peptide substrate. The fluorescence plate reader was calibrated using authentic oxidized Amplex Red (Resorufin) (Molecular Probes) for determination of the stoichiometry of the hMetAP2 reaction. Assays were initiated with the addition of substrate, and the initial rates were corrected for the background rate determined in the absence of hMetAP2.

Direct (Uncoupled) Spectrophotometric Assays of hMetAP2 on a Multiwell Plate Reader. The hMetAP2 activity could also be measured by direct spectrophotometric assay methods using alternative substrates, L-methionine *p*-nitroanilide (Met-pNA) and L-methionine 7-amido-4-methylcoumarin (Met-AMC). The formation of *p*-nitroaniline (pNA) or 7-amido-4-methylcoumarin (AMC) was continuously monitored by increasing absorbance at 405 nm or fluorescence ($\lambda_{ex} = 360$ nm, $\lambda_{em} = 460$ nm), respectively, on a corresponding plate reader. All assays were carried out at 30 °C. The fluorescence or spectrophotometric plate reader was calibrated using authentic pNA or AMC from Sigma, respectively. For a typical 96-well plate assay, the increase in absorbance (at 405 nm for pNA) or the fluorescence emission ($\lambda_{ex} = 360$ nm, $\lambda_{em} = 460$ nm, for AMC) in each well was used to calculate the initial velocity of hMetAP2. Each 50 μL assay contained 50 mM Hepes (pH 7.5), 100 mM NaCl, 10−100 nM purified hMetAP2, and varying amounts of Met-AMC (in 3% DMSO aqueous solution) or Met-pNA. Assays were initiated with the addition of substrate, and the initial rates were corrected for the background rate determined in the absence of hMetAP2.

For divalent metal ions and product inhibition studies, the direct spectrophotometric assay method was employed using the same assay conditions described above. The metal ions, including Co^{2+}, Mg^{2+}, Mn^{2+}, and Zn^{2+} (0.1 μM to 5 mM), were tested in the hMetAP2-catalyzed cleavage of Met-AMC (400 μM). For substrate specificity studies, 13 commercially available amino acid AMC analogues (Phe-, His-, Lys-, Ile-, Leu-, Asn-, Gln-, Arg-, Ser-, Thr-, Val-, Trp-, and Tyr-AMC), in addition to Met-AMC, were used in the hMetAP2-catalyzed reactions. As a control, all these amino amides were first tested in reactions catalyzed by alanine aminopeptidase from bovine intestinal mucosa (Sigma), a nonspecific exopeptidase. The product or product analogues examined as putative inhibitors were L-methionine, L-norleucine (L-Nle), L-methioninesulfone, L-methionine-(*RS*)-sulfoxide, and AMC. Compounds were preincubated with hMetAP2 for 10 min at room temperature before the addition of substrate to initiate the reaction.

Kinetic Data Analysis. Data were fitted to the appropriate rate equations by nonlinear regression using Grafit 4.09 (Erithacus Software). Initial velocity data conforming to Michaelis−Menten kinetics were fitted to eq 5. Inhibition patterns conforming to apparent linear competitive and linear noncompetitive inhibition were fitted to both eqs 6 and 7, respectively, for each inhibitor, and the best fit was determined from the data which yielded the lower residuals.

$$v = VA/(K_a + A) \quad (5)$$

$$v = VA/[K_a(1 + I/K_{is}) + A] \quad (6)$$

$$v = VA/[K_a(1 + I/K_{is}) + A(1 + I/K_{ii})] \quad (7)$$

In eqs 5−7, v is the initial velocity, V is the maximum velocity, K_a is the apparent Michaelis constant, I is the inhibitor concentration, A is the concentration of the variable substrate, and K_{is} and K_{ii} are the apparent slope and intercept inhibition constants, respectively. The nomenclature used in the rate equations for the inhibition constants is that of Cleland (*8*), in which K_{is} and K_{ii} represent the apparent slope and intercept inhibition constants, respectively.

For active site titration or tight-binding inhibition of the full-length and N-terminally truncated hMetAP2 enzymes, the initial rates of the peptidolytic reactions were obtained at variable enzyme concentrations, at changing fixed levels of inhibitor, and at a single fixed concentration of the Met-Gly-Met-Met substrate. The stoichiometry of the functional active site and apparent inhibition constant for a tight-binding inhibitor were obtained by fitting to eq 8 (*1*, *7*, *13*, *25*) as shown below:

$$v_i/v_0 = \{\alpha E_t - I_t - K_i' + [(\alpha E_t - I_t + K_i')^2 + 4K_i' I_t]^{1/2}\}/2\alpha E_t \quad (8)$$

[2] The change in the extinction coefficient at 450 nm upon oxidation of *o*-dianisidine at 30 °C was measured by quantitatively converting a discrete amount of *o*-dianisidine to its oxidized form in the presence of excess H_2O_2 and HRP.

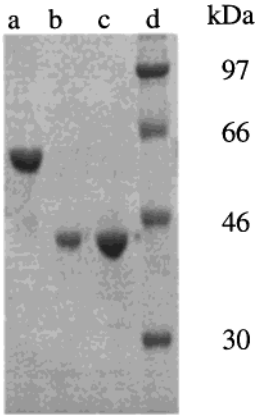

FIGURE 2: Nu−PAGE (10% polyacrylamide, Novex) analysis of purified full-length and N-terminally truncated hMetAP2. Proteins were visualized by staining with Coomassie Blue. Lanes a−d represent approximately 5 μg of full-length hMetAP2 (a), 2 μg of truncated hMetAP2 (b), 5 μg of truncated hMetAP2 (c), and molecular markers (d). The estimated purity of the enzyme samples is >90%.

where v_i and v_0 are the initial velocities in the presence and absence of inhibitor, respectively, α is the fraction of active enzyme, $K_i' = K_i(1 + A/K_a)$ (where K_i is the inhibition constant), A is the fixed substrate concentration, E_t and I_t are the total concentrations of enzyme (based on protein concentration) and inhibitor, respectively.

RESULTS AND DISCUSSION

Physical Properties of Intact and Truncated hMetAP2 Enzymes. Both the full-length and truncated forms of hMetAP2 were expressed and purified to apparent homogeneity (Figure 2). N-Terminal amino acid sequencing as well as MALDI-MS analyses showed that, for the full-length recombinant enzyme of hMetAP2, the N-terminal methionine was removed proteolytically, and the penultimate Ala residue in the sequence was acetylated. For the truncated hMetAP2 enzyme, the N-terminal residue was found to be Gly-108 of the full-length sequence. Molecular masses measured by MALDI-MS for the intact and truncated hMetAP2 forms (52 785 and 41 450 Da, respectively) were consistent with the expected values calculated from the amino acid sequences (52 791.4 and 41 456.3 Da, respectively).

Analytical ultracentrifugation showed that both hMetAP2 forms were apparently monomeric at concentrations up to approximately 100 μM. Sedimentation patterns of both the full-length and truncated proteins were well-described in solution by a single-homogeneous species model with average molecular masses at equilibrium of 54.7 ± 0.2 and 41.7 ± 0.5 kDa, respectively (Figure 3). Circular dichroism spectra showed that both molecules are predominantly well-folded (Figure 4A), and appeared to be similar in their overall secondary structural content. The folding stabilities of the two forms were also compared using guanidinium and urea as denaturants. The denaturation curves for the full-length and truncated forms of hMetAP2 were found to be essentially the same (Figure 4B), thereby indicating that both forms have similar energetics of folding. The deletion of the 107 N-terminal residues from hMetAP2, thus, does not apparently affect the overall structure of the catalytic, C-terminal domain of hMetAP2. This is consistent with the observation from

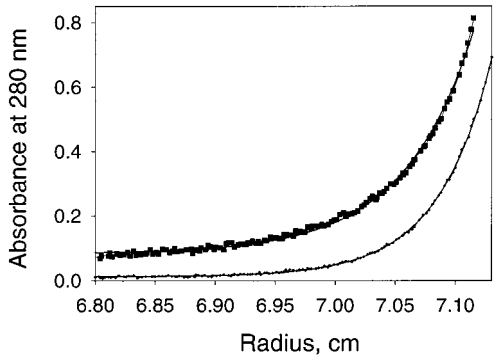

FIGURE 3: Sedimentation equilibrium analysis of the solution masses of full-length (+) and truncated (■) hMetAP2. Best-fit curves are plotted along with the data (Materials and Methods). Nonlinear least-squares fitting to a single-molecular species model yielded solution masses of 54.7 ± 0.2 and 41.7 ± 0.5 kDa for full-length and truncated hMetAP2, respectively. The buffer was 5 mM Hepes and 100 mM NaCl (pH 7.5 and 20 °C). The rotor speed was 22 000 rpm.

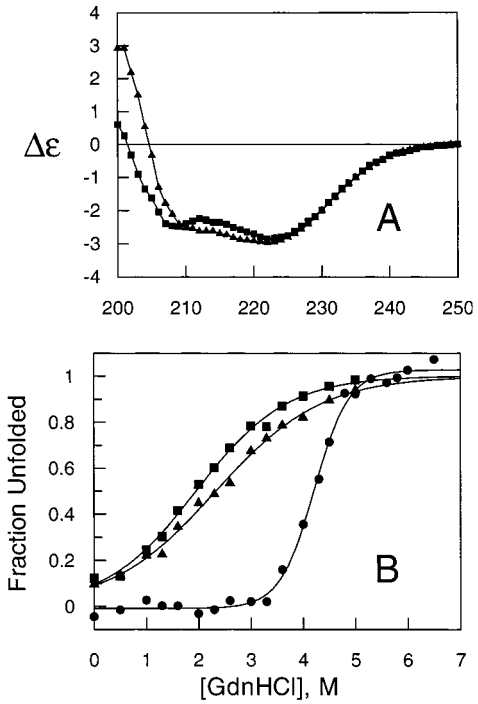

FIGURE 4: Circular dichroism spectra (A) and guanidinium hydrochloride denaturation (B) analyses of full-length (■) and truncated (▲) hMetAP2. CD spectra are shown as molar ellipticity vs wavelength. Best-fit curves are shown for an assumed two-state unfolding model (Eftink, 1995). Guanidinium HCl denaturation data show that both enzyme forms have a broad unfolding transition and have similar folding stabilities. Denaturation of lysozyme (●) is shown for comparison. The conditions included 5 mM HEPES, 100 mM NaCl, pH 7.5, and 20 °C.

the recent crystal structure study of hMetAP2 that the first 109 N-terminal residues of hMetAP2 are disordered and distal to the enzyme active site (*23*). Interestingly, both forms of the enzyme exhibit unusually broad denaturant unfolding curves. The physical origin of this is unknown, but may be due to overlapping of multiple unfolding transitions. To our knowledge, hMetAP2 is the only known monomeric enzyme to have such an unusually broad denaturation transition, a finding that may be related to the unusually high stability of its enzymatic activity. Human MetAP2 can be stored in a

Table 1: Kinetic Parameters of the Full-Length Human Methionine Aminopeptidase (Type 2)[a]

substrate	K_m (mM)	k_{cat} (min^{-1})	k_{cat}/K_m (M^{-1} min^{-1})	relative k_{cat}/K_m
Met-Ala-Ser[b]	0.38 ± 0.03	210 ± 5	(5.5 ± 0.5) × 10^5	100
Met-Gly-Met-Met[b]	0.34 ± 0.04	170 ± 6	(5.1 ± 0.6) × 10^5	93
Met-Leu-Phe[b]	N/A	0.0	0.0	0.0
Met-Ala[b]	∼15	∼7.7	∼5.2 × 10^2	
0.095 Met-Gly[b]	>15	N/A	N/A	N/A
Met-Pro[b]	2.8 ± 0.2	7.8 ± 0.4	(2.7 ± 0.2) × 10^3	0.49
Met-Val[b]	1.2 ± 0.1	0.80 ± 0.02	(6.7 ± 0.6) × 10^2	0.12
Met-Thr[b]	1.3 ± 0.3	0.60 ± 0.06	(4.6 ± 0.1) × 10^2	0.084
Met-Ser[b]	0.85 ± 0.23	0.37 ± 0.04	(4.4 ± 0.1) × 10^2	0.080
Met-Xaa1[b]	N/A	0.0	0.0	0.0
Met-AMC[c]	0.31 ± 0.02	3.3 ± 0.1	(1.1 ± 0.1) × 10^4	2.0
Xaa2-AMC[c]	N/A	0.0	0.0	0.0
Met-pNA[c]	0.67 ± 0.11	9.5 ± 0.3	(1.4 ± 0.2) × 10^4	2.5
Nle-pNA[c]	2.0 ± 0.3	4.4 ± 0.3	(2.2 ± 0.4) × 10^3	0.40

[a] Xaa1, one of the L-amino acids of Asn, Glu, Ile, Leu, Lys, Met, D-Met, Phe, Trp, and Tyr; Xaa2, one of the L-amino acids of Phe, His, Lys, Ile, Leu, Asn, Gln, Arg, Ser, Thr, Val, Trp, and Tyr. Data were fitted to eq 5. [b] AAO/HRP coupling enzyme assay (pH 7.5 and 30 °C). [c] Fluorimetric or spectrophotometric assays (pH 7.5 and 30 °C).

buffer at 4 °C for several months without a significant loss of activity.

Steady-State Kinetics of Peptide and Amino Acid Substrates of hMetAP2. Using the spectrophotometric assay (Materials and Methods), steady-state kinetic analysis was conducted on methionine-AMC (or -pNA) and methionine analogue-AMC (or -pNA) substrates via fluorogenic or chromagenic assays, and on various di- and tripeptide substrates via the fluorogenic coupled-enzyme assay. As expected for a metalloprotease, no burst phase was observed for any progressive curve of product formation reported in this study. The results are summarized in Table 1. Consistent with previous reports on various methionine aminopeptidases, hMetAP2 specifically cleaved the N-terminal L-Met from both Met-Ala-Ser and Met-Gly-Met-Met. When the P1′ amino acid (*31*) of the peptide substrate was sterically large (gyration radius of >1.29 Å), such as with L-Leu, hMetAP2 exhibited no detectable activity (Table 1). It is an interesting and novel finding that hMetAP2 was also able to utilize substrates smaller than a dipeptide, such as Met-AMC and Met-pNA. Both were competent substrates of hMetAP2, albeit with poorer activity than the di- and tripeptides. Human MetAP2 also demonstrated stringent specificity for the residue at the P1 position. Like *E. coli* methionine aminopeptidase (type 1), L-Nle was found to be the only amino acid residue other than L-Met (N-terminally formylated Met-Ala-Ser also serves as a substrate for hMetAP2, unpublished data) that could be accommodated at the N-terminus of a substrate. Thirteen other commercially available amino acid AMC analogues (from Bachem), including Phe, His, Lys, Ile, Leu, Asn, Gln, Arg, Ser, Thr, Val, Trp, and Tyr, were examined and showed no cleavage by hMetAP2. As a control, all of these analogues were active as substrates for alanine aminopeptidase (a nonspecific exopeptidase from bovine intestinal mucosa) (Table 1). These results are consistent with the fact that hMetAP2 contains a stringently specific substrate binding site as shown in the recently determined crystal structure (*23*), as it is highly selective for L-methionine at the N-terminus.

The observed hMetAP2-catalyzed cleavage of Met-AMC and Met-pNA suggests that dipeptidoids of the form Met-Xaa could also be the substrates of the enzyme. *N*-Methionine dipeptides of the form Met-Xaa, in which Xaa includes Ala, Asn, Glu, Gly, Ile, Leu, Lys, Met, D-Met, Phe, Pro, Ser, Thr, Trp, Tyr, and Val, were tested as substrates for hMetAP2 using the coupled assay methods. Due to the fact that 1 mol of dipeptide generates 2 mol of free L-amino acids, the k_{cat} values in Table 1 for the active dipeptides were corrected by a factor of 2. The catalytic efficiencies (k_{cat}/K_m) of the dipeptides were summarized and compared to that of Met-Ala-Ser (relative $k_{cat}/K_m = 100$) in Table 1. In general, the dipeptides that were tested were apparently poorer substrates than the amino acid amide substrates Met-AMC and Met-pNA. As expected, dipeptides in which the residue at P1′ was a small amino acid (Ala, Pro, Ser, etc.) were suitable as substrates, whereas dipeptides bearing larger residues at P1′ were poor substrates. Since the *E. coli* MetAP was found to be only active toward tripeptides or larger substrates (*4*), hMetAP2 clearly has different substrate specificity than the *E. coli* MetAP despite the similar active site structures of the two enzymes.

Scheme 1

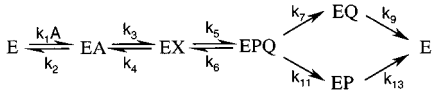

The kinetic parameters of the amino acid amides and di- and tripeptide substrates of full-length hMetAP2 are found in Table 1. The two tri-/tetrapeptide substrates were essentially equivalent in terms of their values of K_m and k_{cat}. For the amino acid amides Met-AMC and Met-pNA, Met-pNA exhibited the higher turnover rate ($k_{cat} = 9.5$ min^{-1}), whereas Met-AMC exhibited the lower Michaelis constant ($K_m = 0.31$ mM), similar to that of the peptide substrates. Nle-pNA displayed an elevated K_m value of 2.0 mM which is comparable to those of the dipeptide substrates.

A minimal mechanistic scheme for a metalloprotease which has a random release of products is shown in Scheme 1. A, P, and Q represent the substrate and two products, respectively, while EX is the adduct of the peptide substrate and water. For the upper pathway, expressions for k_{cat}/K_m, K_m, and V_{max} are shown in eqs 9−11.

$$k_{cat}/K_m = k_1k_3k_5k_7/[k_2k_4(k_6 + k_7) + k_5k_7(k_2 + k_3)] \quad (9)$$

$$k_{cat} = k_3k_5k_7/[(k_3 + k_4)(k_6 + k_7) + k_3k_5k_7(1/k_3 + 1/k_7 + 1/k_9)] \quad (10)$$

$$K_m = [k_2k_4(k_6 + k_7) + (k_2 + k_3)k_5k_7]/\{k_1[(k_3 + k_4)(k_6 + k_7) + k_3k_5k_7(1/k_3 + 1/k_7 + 1/k_9)]\} \quad (11)$$

Modeling studies of the expressions in eq 9−11 indicate that the significant decreases in the relative values of k_{cat}/K_m and k_{cat}, with little change in the values of K_m, for the substrates that were examined (Table 1) undoubtedly arise from decreasing values of either k_3, k_5, or both. The greatly reduced catalytic efficiency (k_{cat}/K_m) of Met-AMC (52-fold lower than that of Met-Ala-Ser, Table 1) as well as Met-pNA (39-fold) is almost entirely due to the reduction in the turnover rate (k_{cat}) which could be consistent with either the formation of the tetrahedral intermediate complex (EX) or its breakdown as being rate-limiting in catalysis.

Table 2: Product Inhibition of Full-Length Human Methionine Aminopeptidase (Type 2)[a]

compound	substrate	inhibition pattern	K_{is} (μM)
L-methionine	Met-AMC	competitive	20 ± 3
AMC	Met-pNA	competitive	290 ± 40
L-norleucine	Met-AMC	competitive	41 ± 6
L-Met-(*RS*)-sulfoxide	Met-AMC	competitive	180 ± 20

[a] Data were fitted to eqs 6 and 7 and best fit was determined from the sum of the least residuals.

As seen in the relative values of k_{cat}/K_m, the active dipeptides displayed less than 0.5% catalytic efficiency compared to the tri- and tetrapeptides, which is manifested in both the elevation in K_m and the decrease in k_{cat} of these substrates. This suggests that the residues at the P2′ position and/or beyond are critical to both the formation of Michaelis complexes and stabilization of transition states in the enzyme active site. Of the active dipeptides, Met-Ala, Met-Pro, Met-Ser, Met-Thr, and Met-Val, the result indicated that relatively small amino acids in the P1′ are the only suitable residues at this position. The similar k_{cat} values for the dipeptides and Met-AMC or Met-pNA suggest that hMetAP2 catalyzes a similar hydrolytic cleavage reaction of amide bonds in peptides and in the alternative substrates. The similar K_m values of Met-AMC and the tri- or tetrapeptides and the ability to directly monitor the AMC release make Met-AMC an ideal substrate in our following mechanistic studies of the enzyme system of hMetAP2 using pH profile and solvent isotope effect methods (manuscript in preparation).

Product Inhibition. Inhibition of hMetAP2 by reaction products, L-Met, AMC, and L-Nle, as well as various methionine-related non-natural amino acids, including L-Met-(*RS*)-sulfoxide, was performed to elucidate in part the kinetic mechanism of the full-length hMetAP2, and to explore the proposed deep binding cleft that apparently accommodates the side chain of L-Met, as suggested by X-ray structures (*23*). Data from product inhibition patterns of inhibitors versus either Met-AMC or Met-pNA are summarized in Table 2, and were fitted to both eqs 6 and 7 to determine the patterns of product inhibition. All compounds that were examined exhibited apparent linear competitive inhibition versus the substrate Met-AMC (and Met-pNA for AMC) (Table 2). The fact that both L-methionine and AMC exhibited competitive inhibition with the inhibition constants K_{is}(Met) of 20 μM and K_{is}(AMC) of 290 μM indicates a likely random uni-bi kinetic mechanism for the hMetAP2 enzyme (as depicted in Scheme 1). The 10-fold greater binding affinity of L-Met compared to that of AMC in the active site of hMetAP2 further supports the possibility that L-Met is the key anchor for the binding of the substrate. As expected, K_{is} values for the substrate analogues, L-Nle and L-Met-sulfoxide, were greater than that of methionine (41 and 180 μM, respectively). The 2−10-fold increase in the inhibition constants of the L-methionine (Table 2) suggests that, as expected, the side chain of methionine plays an important role in the binding of substrate in the active site of hMetAP2. The sulfur atom and its position in the side chain of L-Met also appear to be crucial in substrate−enzyme recognition. The difference in the K_{is} values of L-norleucine and L-methionine matches well with the observed differences in the K_m values of Nle-pNA and Met-pNA (Table 1).

Table 3: Kinetic Parameters of the Truncated Human Methionine Aminopeptidase (Type 2)

substrate	K_m (mM)	k_{cat} (min^{-1})	k_{cat}/K_m (M^{-1} min^{-1})
Met-Ala-Ser[a]	0.30 ± 0.03	97 ± 2	$(3.2 \pm 0.3) \times 10^5$
Met-Gly-Met-Met[a]	0.36 ± 0.06	120 ± 9	$(3.3 \pm 0.6) \times 10^5$
Met-AMC[b]	0.58 ± 0.04	1.3 ± 0.04	$(2.2 \pm 0.1) \times 10^3$
Met-pNA[b]	0.47 ± 0.05	4.8 ± 0.2	$(1.0 \pm 0.1) \times 10^4$
Nle-pNA[b]	2.1 ± 0.3	1.8 ± 0.2	$(8.6 \pm 1.5) \times 10^2$

[a] Measured by the AAO/HRP coupled enzyme assay. [b] Measured by the direct spectrophotometric assay at pH 7.5 and 30 °C. Data were fitted to eq 5.

Kinetic Comparison of the Truncated hMetAP2 Enzyme. For yeast methionine aminopeptidase (Type 1), its N-terminal extension (zinc finger domain) was shown to be dispensable for the methionine aminopeptidase activity (*41*). The N-terminal truncated yeast MetAP1 enzyme exhibited essentially the same K_m and k_{cat} values as the full-length enzyme. The N-terminal extension (acidic and basic residue clusters) of hMetAP2 was postulated to be involved only in protein−protein recognition with the eukaryotic initiation factor 2α (*14*). In this study, we prepared a truncated hMetAP2 enzyme by limited proteolysis of the intact hMetAP2, whose N-terminal sequence begins at Gly-108 (Materials and Methods). Recently, the same N-terminally truncated hMetAP2 was subcloned, overexpressed, and purified in-house. The truncated hMetAP2 generated by two different methods yielded identical kinetic behavior and physical properties (G. Yang et al., unpublished results).

As discussed earlier, the truncated hMetAP2 appeared to have physical properties very similar to those of the full-length hMetAP2. The same spectrophotometric assays were used to characterize the truncated hMetAP2 enzyme, and kinetic results are summarized in Table 3. The K_m values of all competent substrates of the truncated hMetAP2 were essentially the same as those of the intact, wild-type enzyme, whereas the turnover rates were 2−3-fold lower than those of the full-length hMetAP2 (Tables 1 and 3), assuming that both enzymes are 100% active. The same steady-state affinity (K_m value) for both truncated and intact hMetAP2 enzymes indicates that the removal of the N-terminal portion of wild-type hMetAP2 does not adversely affect the ability of hMetAP2 to form the Michaelis complex in the active site. The same observed reduction (2−3-fold) in k_{cat} values for all the substrates that were examined suggests that the fraction of active enzyme of the truncated hMetAP2 could be ≤50% of that of the full-length wild-type enzyme. This was verified by the stoichiometric titration of the active hMetAP2 for both the full-length and truncated hMetAP2 using the methods of Ackermann and Potter (*1*), Morrison (*25*), and Cha (*7*) (Figure 5). A known active site irreversible inhibitor, fumagillin (Sigma, >90% pure), was used to titrate the active sites of both enzymes. From the analysis, 110 ± 10% of the active sites of the full-length hMetAP2 are shown to be functional, whereas only 73 ± 7% of the active sites within the homogeneous N-terminally truncated hMetAP2 (Figure 5) are functional, consistent with the apparent loss of activity (k_{cat}) of the truncated enzyme. The apparent K_i values of fumagillin for the full-length and truncated hMetAP2 appeared to be the same (1.6 ± 0.2 and 1.2 ± 0.2 nM, respectively).

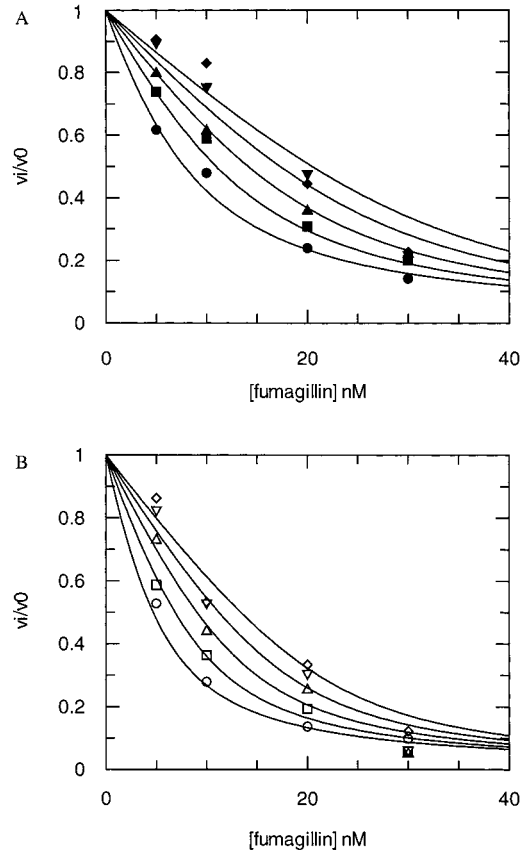

FIGURE 5: Active site titration of full-length and truncated hMetAP2 using a known irreversible active site inhibitor, fumagillin, with Met-Gly-Met-Met as the substrate. Peptidolytic activity at 0.4 mM Met-Gly-Met-Met was measured by the AAO/HRP coupled assay method at variable concentrations of hMetAP2 (6−30 nM) and at changing fixed levels of inhibitor (0−30 nM) in HEPES buffer (pH 7.5) containing 100 mM NaCl and 10 μM $CoCl_2$ at 30 °C. The curves drawn through the experimental data points were generated by fitting the data to eq 8. (A) Titration of the full-length hMetAP2 at 6 (●), 12 (■), 18 (▲), 24 (▼), and 30 nM enzyme (◆). (B) Titration of the N-terminally truncated hMetAP2 at 6 (○), 12 (□), 18 (△), 24 (▽), and 30 nM enzyme (◇).

Table 4: Effect of Exogenous Addition of Divalent Cations on the Full-Length hMetAP2 Enzyme (pH 7.5 and 30 °C)[a]

treatment	relative activity (%)	treatment	relative activity (%)
no addition	100	5.0 mM $MgCl_2$	75
0.1 mM $CoCl_2$	83	0.1 mM $MnCl_2$	74
1.0 mM $CoCl_2$	42	1.0 mM $MnCl_2$	78
0.1 mM $MgCl_2$	83	5.0 mM $MnCl_2$	64
1.0 mM $MgCl_2$	79	0.1 mM $ZnCl_2$	0.2

[a] Relative enzymatic activities were determined using Met-AMC (400 μM) as a substrate. Control samples assayed under the same conditions (with no additions) were considered to be 100% activity. The estimated errors are ±10%.

Effect of Divalent Metal Cations. Table 4 summarizes the effects of added Co^{2+}, Mg^{2+}, Mn^{2+}, and Zn^{2+} on hMetAP2 activity. Assays were carried out using the direct spectrophotometric method with Met-AMC as the substrate (Materials and Methods). The control sample (no added metal ions) contained a baseline concentration of Co(II) of 0.1 μM. It appears that all the metal cations that were examined showed a certain degree of inhibition on the full-length hMetAP2-catalyzed hydrolysis of Met-AMC (Table 4). Unlike the previous reports (*22*), in which a noncontinuous assay method was employed, no enhancement of the catalytic activity of hMetAP2 was observed upon addition of ≥100 μM exogenous divalent metal cations. Excess Co^{2+} appeared to inhibit the enzyme activity with an IC_{50} value of ∼1 mM. Zinc cation completely inactivated hMetAP2 at a concentration of 0.1 mM. Excess Mn^{2+} and Mg^{2+} appeared to have a non-dose-dependent effect on the activity of hMetAP2, indicating that they are likely not kinetically relevant. Since the type 1 yeast MetAP enzyme was suggested to use Zn^{2+} instead of Co^{2+} as its metal cofactor under physiological conditions (*36*), we decided to further examine the inhibitory effects of Zn(II) on hMetAP2.

Table 5: Effect of Co^{2+} and Zn^{2+} on the Kinetic Parameters of Full-Length Human Methionine Aminopeptidase (Type 2) (pH 7.5 and 30 °C) Using Met-AMC as a Substrate[a]

metal cation	K_m (mM)	k_{cat} (min^{-1})	k_{cat}/K_m (M^{-1} min^{-1})
no metal	0.27 ± 0.03	0.88 ± 0.04	(3.3 ± 0.1) × 10^3
0.1 μM $CoCl_2$	0.21 ± 0.03	1.0 ± 0.05	(4.8 ± 0.7) × 10^3
1.0 μM $CoCl_2$	0.18 ± 0.03	2.0 ± 0.1	(1.1 ± 0.2) × 10^4
10 μM $CoCl_2$	0.12 ± 0.02	3.8 ± 0.2	(3.2 ± 0.6) × 10^4
0.1 μM $ZnCl_2$	0.24 ± 0.03	0.73 ± 0.03	(3.0 ± 0.2) × 10^3
1.0 μM $ZnCl_2$	0.22 ± 0.03	0.16 ± 0.01	(7.3 ± 1.1) × 10^2
10 μM $ZnCl_2$	−	inactive	−

[a] Data were fitted to eq 5.

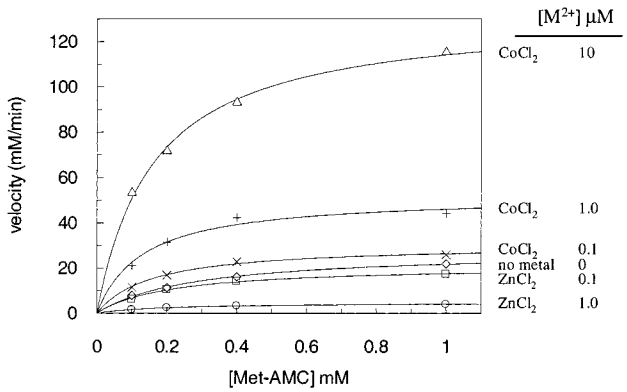

FIGURE 6: Velocity vs [S] plot of hMetAP2-catalyzed hydrolysis of Met-AMC in the presence of 10 μM $CoCl_2$ (△), 1.0 μM $CoCl_2$ (+), 0.1 μM $CoCl_2$ (×), 0 μM metal ions (◇), 0.1 μM $ZnCl_2$ (□), and 1.0 μM $ZnCl_2$ (○). Reactions were carried out at pH 7.5 and 30 °C as described in Materials and Methods.

To minimize the exogenous metal ions introduced during the enzyme expression and purification [normally, 0.5 mM Co(II) was added during column chromatography], the recombinant hMetAP2 was overexpressed and purified in the absence of any exogenous divalent metal cations (except endogenous amounts in the cell growth medium). The Co(II) and Zn(II) content of the purified hMetAP2 was quantitated by ICP emission analysis (detection limit of 0.08 ppm). No detectable Co(II) was found, whereas stoichiometric amounts (0.78 ppm) of Zn(II) {1:1 [hMetAP2]:[Zn(II)]} were detected in the enzyme sample. The purified hMetAP2 was then tested for enzymatic activity in the presence of 0−10 μM $CoCl_2$ or $ZnCl_2$ (final assay concentration) using the direct spectrophotometric assay method with MetAMC as the substrate (Table 5 and Figure 6). The apoenzyme showed detectable activity even in the absence of any additional divalent metal cations. No stimulation of hMetAP2 activity was observed with stoichiometric addition of $ZnCl_2$ (100 nM $ZnCl_2$ vs 70 nM enzyme), and at 1.0 μM

$ZnCl_2$, the enzyme lost 78% of its original activity (Figure 6). $CoCl_2$, on the other hand, clearly enhanced the methionine aminopeptidase activity of hMetAP2 at a concentration as low as 100 nM (1 equiv) (Figure 6). However, unlike the observation for the *E. coli* MetAP (*10*), 1 equiv of Co(II) apparently was not sufficient to activate the hMetAP2 enzyme to its optimal activity, suggesting that 2 equiv of metal ions is most likely required for hMetAP2 to be fully functional (at least in vitro). From crystallographic data of hMetAP2 (*23*), one tightly bound and one loosely bound Co(II) ion were clearly seen in the metal center of the active site of hMetAP2. At 10 μM $CoCl_2$ [100 equiv, which could reflect the relatively weak association of the loosely bound Co(II) ion in the hMetAP2 active site], the enzyme appeared to reach its optimal activity (10-fold elevation of the baseline activity). The baseline hMetAP2 activity that is observed, thus, is not a result of lack of an additional 1 equiv of Zn(II) in the enzyme active site. The 1 equiv of Zn(II) associated with hMetAP2 during expression and purification is most likely not due to a requirement of the enzyme active site but bound external to the active site. This is consistent with our current crystallography data that a second metal binding site was observed near the surface of a MetAP enzyme (unpublished result). The observed baseline hMetAP2 activity can be explained by the $<^1/_{10}$ equiv of Co(II) in the enzyme active site which is below the detection limit of ICP analysis. It is worth noting that addition of metal ions [either Co(II) or Zn(II)] had little effect on the K_m value of Met-AMC (Table 5 and Figure 5). Our data clearly support the fact that at a low concentration ($\leq$10 μM), cobalt ions play a key role in the stimulation of the activity of hMetAP2. Although it is still questionable that Co(II) is the physiologically relevant divalent cation in hMetAP2, Zn(II) clearly is not the kinetically relevant divalent cation for hMetAP2. The observed inhibitory effect of Zn^{2+} upon hMetAP2 could be a result of modification of an essential active site residue. It was proposed that Zn(II) was able to modify the key active site Cys residues in the *E. coli* MetAP enzyme to inhibit its catalytic activity (*10*).

Summary. As previously discussed, the exopeptidase activity of the type 2 human methionine aminopeptidase has been implicated to be directly involved in the regulation of growth factor-stimulated endothelial cell proliferation. Complementary to the in vitro results which showed that the binding of fumagillin in hMetAP2 did not impair the association of the N-terminal region of hMetAP2 with the initiation factor (eIF-2α) (*15*), the proteolytic scission of the N-terminal region of the enzyme also did not significantly alter the kinetic behavior of hMetAP2 and the binding affinity of inhibitors of hMetAP2, such as fumagillin, etc., in the enzyme active site. The study presented here provides a kinetic basis for further understanding the reaction mechanism of this important enzyme. Like that of many other metal-containing amidases, such as stromelysin (*16*), thermolysin (*19*), and dapE- and argE-encoded desuccinylase (*6*) and deacetylase (*20*), the catalysis of hMetAP2 is apparently metal ion-dependent and follows a random uni-bi kinetic mechanism. In addition to the common substrate specificity for methionine aminopeptidases, hMetAP2 displays a broader substrate selectivity and an apparently different requirement for the metal center. The fluorogenic compound, Met-AMC, an alternative substrate for hMetAP2, appears to have the same steady-state affinity (K_m) as that of the peptide substrates. The true identity of the metal center in hMetAP2 under physiological conditions remains to be established. Our results appear to exclude the Zn(II) cation as the potential metal cofactor for hMetAP2. The existence of cobalt transporter proteins (*21*) and other transporters for a broad range of divalent cations (Zn^{2+}, Ni^{2+}, and Cd^{2+}) (*26*) in microorganisms suggests that the metal uptake in mammalian cells could be complex, which makes the search for the true physiological metal cation in hMetAP2 more compelling. Due to the current analytical limitation, the target metal-containing protein often needs to be overexpressed in a host cell. The overexpressed recombinant MetAP enzymes may not be tightly regulated by the host. As a result, the metal ion content thus found in the recombinant enzymes could be a reflection of the uptake of the most abundant metal cation in host cells. Genomic mapping for identifying the metal transporter genes whose expression is regulated by the expression of MetAP genes will certainly shed light on this issue, which could provide new therapeutic indications as well as a better understanding of the molecular mechanism of hMetAP2 in cell cycle regulation.

ACKNOWLEDGMENT

We thank Drs. Ricardo Macarron and Murray J. Brown for reviewing the manuscript and for many helpful comments, Ms. Nicole Robertson and Mr. Gilbert Scott for performing amino acid composition, amino-terminal sequencing, and MALDI-MS analysis, and Mr. Thomas C. Potter and Dr. Stephen A. Carr of the Analytical Department for ICP emission spectroscopy. We also acknowledge Dr. Yie-Hwa Chang and St. Louis University as the source of the intellectual property of the type 2 human methionine aminopeptidase.

REFERENCES

1. Ackermann, W. W., and Potter, V. A. (1949*) Proc. Soc. Exp. Biol. Med. 72*, 1.
2. Arfin, S. M., Kendall, R. L., Hall, L., Weaver, L. H., Stewart, A. E., Matthews, B. W., and Bradshaw, R. A. (1995) *Proc. Natl. Acad. Sci. U.S.A. 92*, 7714.
3. Bazan, J. F., Weaver, L. H., Roderick, S. L., Huber, R., and Matthews, B. W. (1994) *Proc. Natl. Acad. Sci. U.S.A. 91*, 2473.
4. Ben-Bassat, A., Bauer, K., Chang, S.-Y., Myambo, K., Boosman, A., and Chang, S. (1987*) J. Bacteriol. 169*, 751.
5. Boissel, J. P., Kasper, T. J., and Bunn, H. F. (1988) *J. Biol. Chem. 263*, 8443.
6. Born, T. L., Zheng, R., and Blanchard, J. S. (1998) *Biochemistry 37*, 10478.
7. Cha, S. (1975) *Biochem. Pharmacol. 24*, 2177.
8. Cleland, W. W. (1963) *Biochim. Biophys. Acta 67*, 104.
9. D'souza, M. D., and Holz, R. C. (1999) *Biochemistry 38*, 11079.
10. D'souza, M. D., Bennett, B., Copik, A. J., and Holz, R. C. (2000) *Biochemistry 39*, 3817.
11. Doyle, M. L., and Hensley, P. (1997) *Adv. Mol. Cell Biol. 22A*, 279.
12. Folkman, J. (1971) *N. Engl. J. Med. 285*, 1182.
13. Grant, S. K., Deckman, I. C., Minnich, M. D., Culp, J., Franklin, S., Dreyer, G. B., Tomaszek, T. A., Jr., Debouck, C., and Meek, T. D. (1991) *Biochemistry 30*, 8424.
14. Griffith, E. C., Su, Z., Turk, B. E., Chen, S., Chang, Y. H., Wu, Z., Biemann, K., and Liu, J. O. (1997) *Chem. Biol. 4* (6), 461.

15. Gupta, N. K., Datta, B., Ray, M. K., and Ray, A. L. (1993) in *Translational Regulation of Gene Expression* (Ilan, J., Ed.) Vol. 2, pp 405−431, Plenum Press, New York.
16. Harrison, R. K., Chang, B., Niedzwiecki, L., and Stein, R. L. (1992) *Biochemistry 31*, 10757.
17. Huang, S., Elliott, R. C., Liu, P.-S., Koduri, R. K., Weickmann, J. L., Lee, J.-H., Blair, L. C., Ghosh-Dastidar, P., Bradshaw, R. A., Bryan, K. M., Einarson, B., Kendall, R. L., Kolacz, K. H., and Saito, K. (1987) *Biochemistry 26*, 8242.
18. Ingber, D., Fujita, T., Kishimoto, S., Sudo, K., Kanamaru, T., Brem, H., and Folkman, J. (1990) *Nature 348*, 555.
19. Izquierdo, M. C., and Stein, R. L. (1990) *J. Am. Chem. Soc. 112*, 6054.
20. Javid-Majd, F., and Blanchard, J. S. (2000) *Biochemistry 39*, 1285.
21. Komeda, H., Kobayashi, M., and Shimizu, S. (1997) *Proc. Natl. Acad. Sci. U.S.A. 94*, 36.
22. Li, X., and Chang, Y.-H. (1996) *Biochem. Biophys. Res. Commun. 227*, 152.
23. Liu, S., Widom, J., Kemp, C. W., Crews, C. M., and Clardy, J. (1998) *Science 282*, 1324.
24. Lowther, W. T., Orville, A. M., Madden, D. T., Lim, S., Rich, D. H., and Matthews, B. W. (1999) *Biochemistry 38*, 7678.
25. Morrison, J. F. (1969) *Biochim. Biophys. Acta 185*, 269.
26. Nies, D. H., and Silver, S. (1989) *J. Bacteriol. 171*, 4073.
27. O'Reilly, M. S., Holmgren, L., Shing, Y., Chen, C., Rosenthal, R. A., Moses, M., Lane, W. S., Cao, Y., Sage, E. H., and Folkman, J. (1994) *Cell 79*, 315.
28. O'Reilly, M. S., Boehm, T., Shing, Y., Fukai, N., Vasios, G., Lane, W. S., Flynn, E., Birkhead, J. R., Olsen, B. R., and Folkman, J. (1997) *Cell 88*, 277.
29. Pace, C. N., Vajdos, F., Fee, L., Grimsley, G., and Gray, T. (1995) *Protein Sci. 4*, 2411.
30. Rijkers, D. T. S., Adams, H. P. H. M., Hemker, H. C., and Tesser, G. I. (1995) *Tetrahedron 51*, 11235.
31. Schechter, I., and Berger, A. (1967) *Biochem. Biophys. Res. Commun. 27* (2), 157.
32. Sherman, F., Stewart, J. W., and Tsunasawa, S. (1985) *BioEssays 3*, 27.
33. Sin, N., Meng, L., Wang, M. Q. W., Wen, J. J., Bornmann, W. G., and Crews, C. M. (1997) *Proc. Natl. Acad. Sci. U.S.A. 94*, 6099.
34. Tahirov, T. H., Oki, H., Tsukihara, T., Ogasahara, K., Yutani, K., Ogata, K., Izu, Y., and Tsunasawa, S. (1998) *J. Mol. Biol. 284* (1), 101.
35. Tsunasawa, S., Izu, Y., Miyagi, M., and Kato, I. (1997) *J. Biochem. 122*, 843.
36. Walker, K. W., and Bradshaw, R. A. (1998) *Protein Sci. 7*, 2684.
37. Wang, J., Quan, N., and Henkin, J. (1998) *Proc. Am. Assoc. Cancer Res. 39*, 98.
38. Woody, R. W. (1995) *Methods Enzymol. 246*, 34.
39. Wu, S., Gupta, S., Chatterjee, N., Hileman, R. E., Kinzy, T. G., Denslow, N. D., Merrick, W. C., Chakrabarti, D., Osterman, J. C., and Gupta, N. K. (1993) *J. Biol. Chem. 268*, 10796.
40. Zhou, M., Diwu, Z., Panchuk-Voloshina, N., and Haugland, R. P. (1997) *Anal. Biochem. 253*, 162.
41. Zou, S., Guo, Q., Ling, C., and Chang, Y.-H. (1995) *Mol. Gen. Genet. 246*, 247.

BI010806R